Electronic Supplementary Material (ESI) for Inorganic Chemistry Frontiers.

Supplementary Information

Durable polymer solar cells produced by encapsulation of WSe_2 hole-transport layer and β-Carotene as active layer additive

Xuan Zheng[a*], ***Xin Miao***[a], ***Yufei Xiao***[a], ***Lei Guo***[a], ***Yalin Wang***[a], ***Tao Hu***[a], ***Xinghou Gong***[a], ***Chonggang Wu***[a], ***Chuanxi Xiong***[b]

[a] *Hubei Provincial Key Laboratory of Green Materials for Light Industry, Collaborative Innovation Center of Green Lightweight Materials and Processing, and School of Materials and Chemical Engineering, Hubei University of Technology, Wuhan, 430068, China*

[b] *State Key Laboratory of Advanced Technology for Materials Synthesis and Processing, Wuhan University of Technology, Wuhan, 430070, China*

E-mail address: zx88@hbut.edu.cn

EXPERIMENTAL SECTION

1 Methods

1.1 Liquid-phase exfoliation of WSe_2

100 mg of bulk WSe_2 powders (5 um, purity>98 %, Sigma-Aldrich) were dispersed in the NaOH/urea (molar ratio = 1 : 2) dispersion. After that, 200 mL of the WSe_2 dispersion were moved to a 500 mL glass beaker, where WSe_2 powders were exfoliated and dispersed via pure mechanical stirring at speed of 1200 rpm for 24 h. Besides, the acquired products were divided equally to 50 ml centrifugal tubes, then maintained at 3000 rpm for 15 min. Take advantage of the top half of the dispersion and re-mixed in DMF, subsequently clearing in ultrasonic baths and filtration with abundant DMF, deionized water and ethanol. Finally removed excess solvents in vacuum oven at 50 ^{o}C. The yield of WSe_2 nanoflakes (NF-WSe_2) was figured by eliminating the mass of the residual solid.

1.2 PSCs fabrication

Glass/ITO substrates (resistance = 20 Ω/sq) were thoroughly washed by ultrasonic machine in deionized water, anhydrous ethanol, acetone, and isopropyl alcohol, respectively. After that, the abluent substrates were uncovered in ultraviolet-ozone chamber for 20 min. In view of the structure and fabrication of PSCs, the 0.5 mg ml^{-1} dispersion (IPA) of NF-WSe_2 was spin coated at 1000 rpm for 30 s for limited times to fulfil the stated thickness without other treatment. Besides, PEDOT:PSS (Clevios 4083) was spin coated onto Glass/ITO at 6000 rpm for 60 s and annealed at 150 °C for 5 min in air to form a 40 nm thick film. The processed substrates were all moved into a glovebox. 100 nm thick PCDTBT: $PC_{71}BM$+bCar active layer was achieved by casting 15 mg mL^{-1} solution (PCDTBT: $PC_{71}BM$ = 1:4 by wt., dissolved in 1, 2-dichlorobenzene with 3 wt. % bCar) at 1400 rpm. Additionally, 90 nm thick PBDB-T: $PC_{71}BM$+bCar active layer was also achieved by casting 20 mg mL^{-1} solution (PCDTBT: $PC_{71}BM$ = 2: 3 by wt., dissolved in 1, 2-dichlorobenzene with 3 wt. % bCar) at 1100 rpm, and treated by thermal annealing at 150 ^{o}C for 10 min. Then, the devices were stored in a glovebox-embedded thermal evaporator and pumped under a background pressure of 2 × 10^{-6} Torr. At last, a layer of 10 nm Ca and 100 nm thick Ag were thermally deposited as the top electrode through shadow masks by thermal evaporation.

2 Measurements and characterization

The crystallographic planes of related samples were characterized using powder X-Ray diffraction (PXRD) with Cu Ka radiation (λ =1.54060 Å). The high-resolution transmission electron microscopy (HRTEM) images were taken on JEM-2100F at 200 kV accelerating voltage. Elemental mapping and EDS were performed with JSM-5160LV-Vantage typed energy spectrometer. The morphology image was obtained by

a SEM (Hitachi SU8010). X-ray photoelectron spectroscopy (XPS) spectra were obtained with a Ulvac-PHI5000 Versaprobe III spectrometer using a Al k source (1486.6 eV). Film thickness was measured using a spectroscopic ellipsometer (J. A. Woollam, USA). The electronic properties of all films were characterized by ultraviolet photoelectron spectroscopy (UPS) using the He I (21.22 eV) excitation line. The Raman spectra were collected using a HORIBA XploRA plus system with a 633 nm laser. Thermogravimetric analysis and differential scanning calorimetry (TG-DSC) was collected using a TA SDT-Q600 with a heating rate of 10 °C/min from 25 to 800 °C in air flow. The UV-absorption spectra of the WSe_2 dispersion were recorded on a spectrophotometer (Shimadzu UV-2550). AFM images were taken on a Bruker Dimension® Icon Scanning Probe Microscope.

The current density-voltage (*J–V*) cuves of the devices were measured with Keithley 2450 source meter unit under 1 sun, the simulated AM 1.5G illumination from a xenon solar simulator (Newport) in air. The light intensity was calibrated with a standard newport standard silicon photovoltaic reference cell. The external quantum efficiency (EQE) measurements were obtained from a QE-3011 system with Newport standard Si diode. Impedance spectra were performed with a PARSTAT 4000A potentiostation and coupled with the Modulab ECS software. The Impedance spectroscopy (IS) data were recorded in the frequency of 1 Hz to 100 kHz by a 10 mV perturbation under dark.

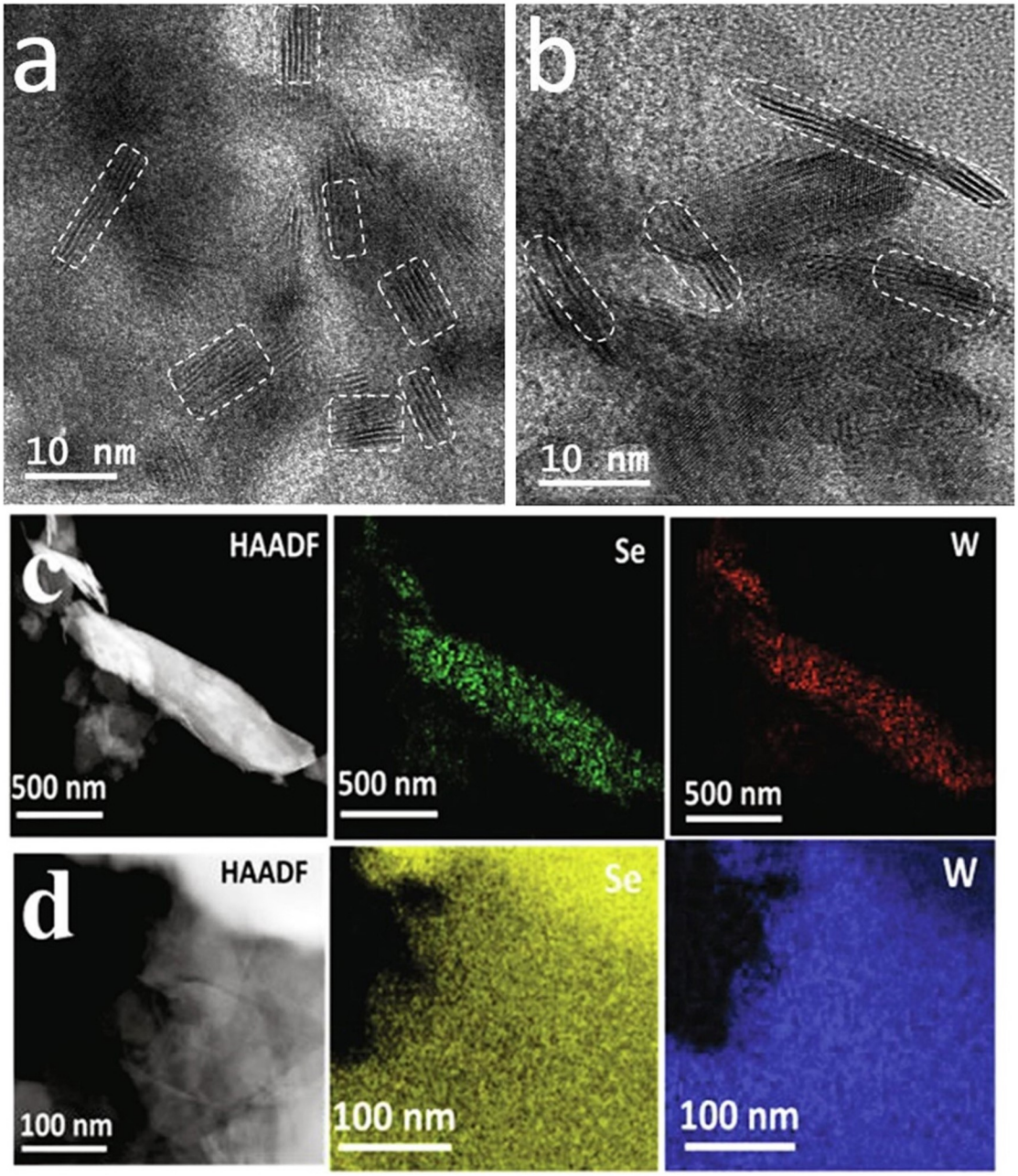

Fig. s1. TEM images of obtained NF-WSe_2 nanocrystals (a, b). The HAADF images of obtained NF-WSe_2 and elemental mapping of Se and W, obtained via EDS (c, d).

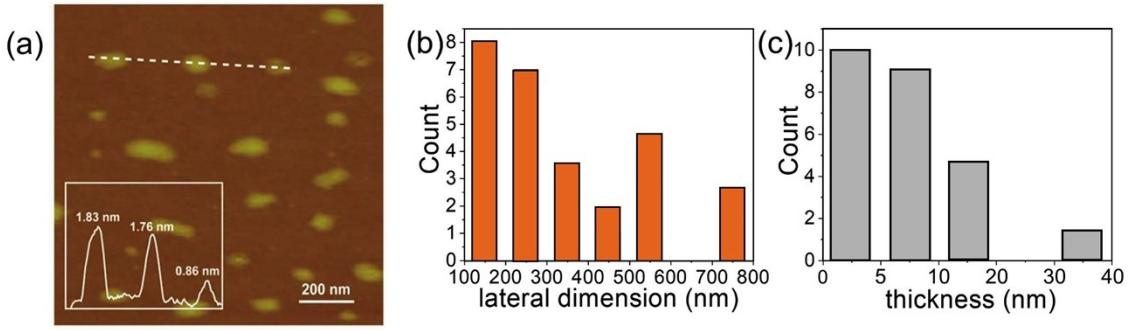

Fig. s2. AFM image of obtained NF-WSe_2 nanocrystals (a). Insets: cross section height profiles. Lateral dimension (b) and thickness (c) distributions of NF-WSe_2 flakes extracted from (a).

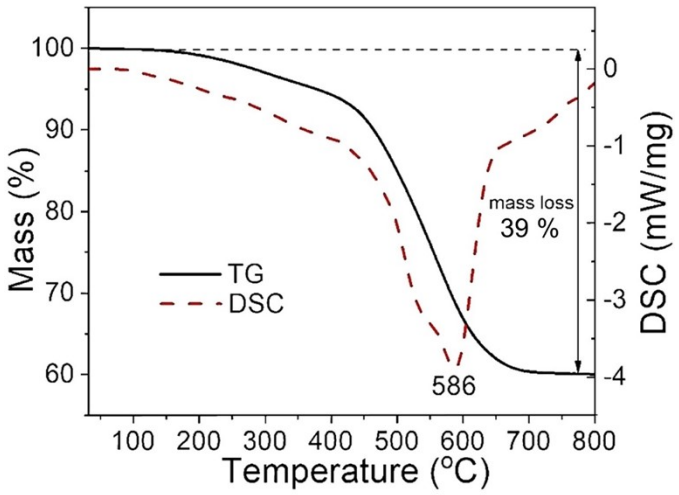

Fig. s3. TG-DSC curves of NF-WSe_2 in an air atmosphere. The thermal stability of NF-WSe_2 in air was confirmed by TG-DSC analysis from room temperature to 800 °C under air. As displayed in Fig. S3, the conversion of WSe_2 revised the maximum exothermic peak at about 586 °C and the final mass loss of 39 %. The decline is caused by the oxidation of NF-WSe_2 to solid WO_3 and gaseous SeO_2.

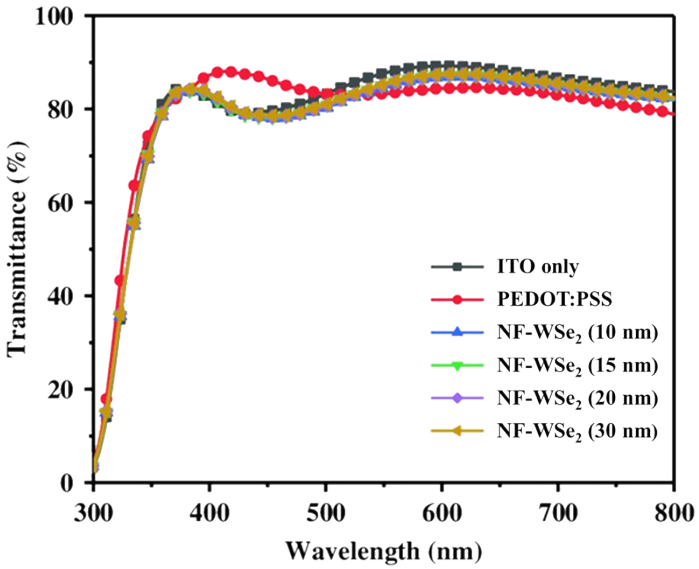

Fig. s4. Transmittance spectra of ITO/glass, PEDOT:PSS/ITO/glass and NF-WSe_2/ITO/glass at various spin-coated thicknesses.

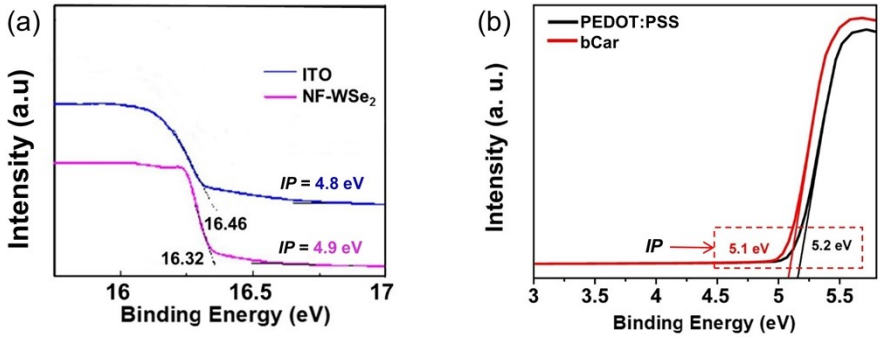

Fig. s5. (a) UPS spectra of the secondary electron cut-off regions of bare ITO and NF-WSe_2 and the corresponding Ionization potentials (*IP*). (b) *IP* curves of PEDOT:PSS and bCar transformed from UPS measurement.

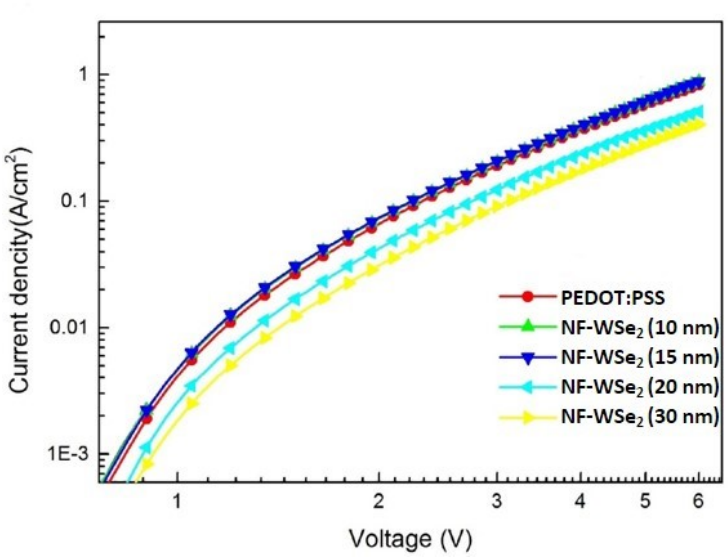

Fig. s6. *J–V* curves of hole-only devices with the configuration of ITO/NF-WSe_2 or PEDOT:PSS/PCDTBT:$PC_{71}BM$+bCar/MoO_3/Ag.

Table s1. Hole mobility of the hole-only devices calculated by the SCLC method.

Devices	**Hole mobility μ_h ($cm^2 V^{-1} s^{-1}$)**
ITO/PEDOT:PSS/PCDTBT:$PC_{71}BM$+bCar/MoO_3/Ag	1.33×10^{-4}
ITO/NF-WSe_2 (10 nm) /PCDTBT:$PC_{71}BM$+bCar/MoO_3/Ag	1.25×10^{-4}
ITO/NF-WSe_2 (15 nm) /PCDTBT:$PC_{71}BM$+bCar/MoO_3/Ag	1.21×10^{-4}
ITO/NF-WSe_2 (20 nm) /PCDTBT:$PC_{71}BM$+bCar/MoO_3/Ag	7.68×10^{-5}
ITO/NF-WSe_2 (30 nm) /PCDTBT:$PC_{71}BM$+bCar/MoO_3/Ag	6.52×10^{-5}

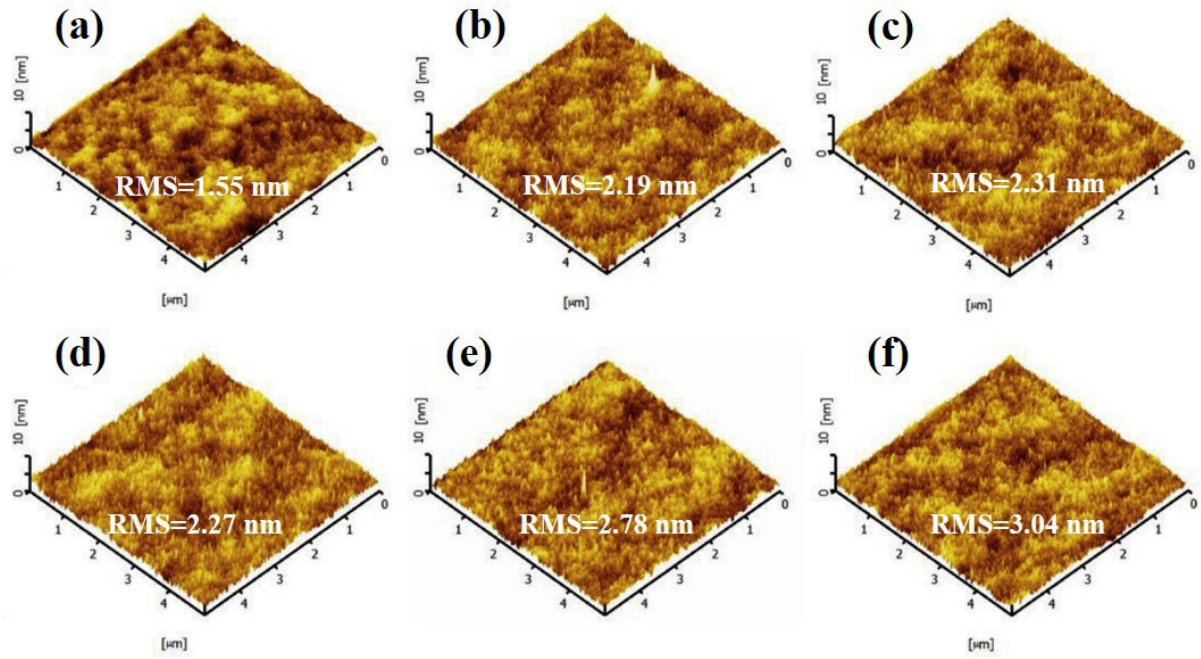

Fig. s7. AFM images as tapping-mode topography of ITO(a) , ITO/PEDOT:PSS(b), ITO/NF-WSe_2(10 nm) (c), (15 nm) (d), (20 nm) (e), (30 nm) (f).

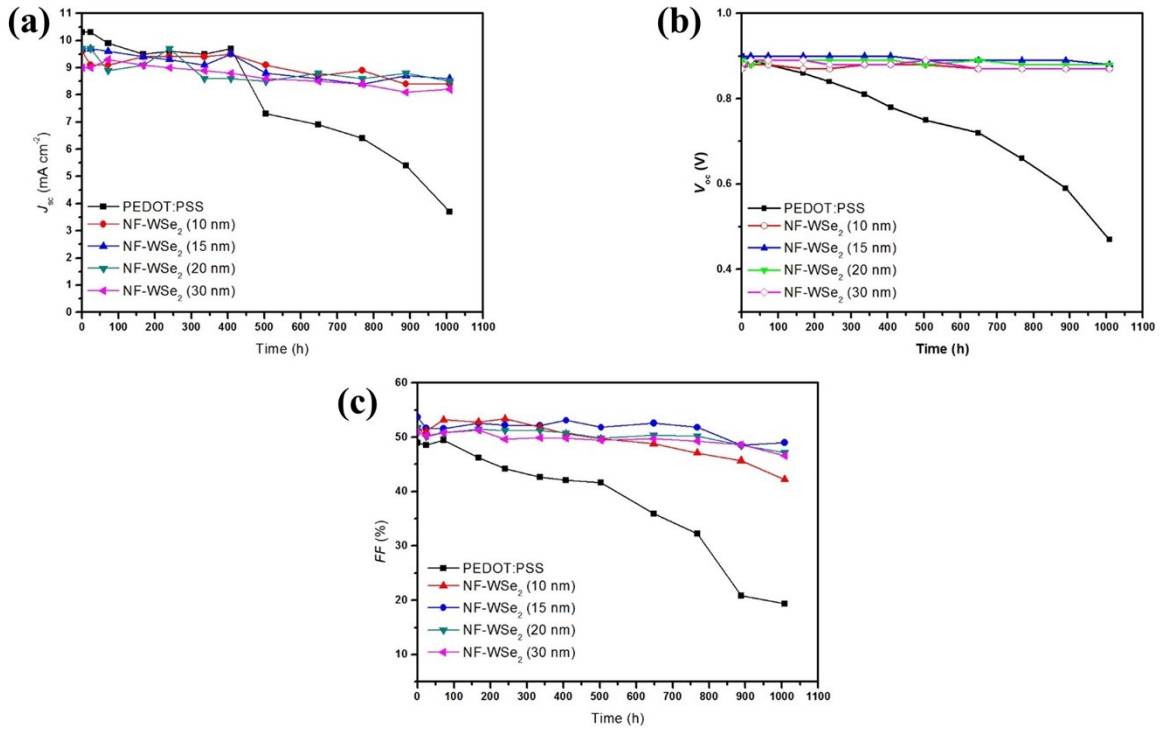

Fig. s8. Long term stability analysis of key photovoltaic parameters (J_{sc}, V_{oc}, and *FF*) of PSCs with PEDOT:PSS and NF-WSe_2 at various spin-coated thicknesses.

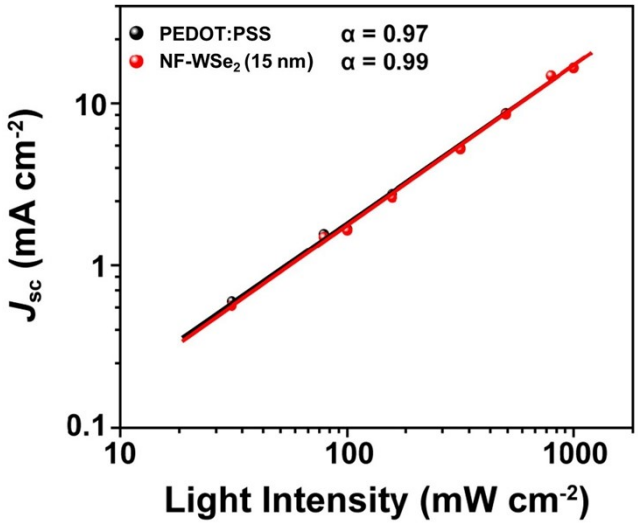

Fig. s9. J_{sc} as a function of light intensity for devices with PEDOT:PSS and NF-WSe_2 (15 nm)

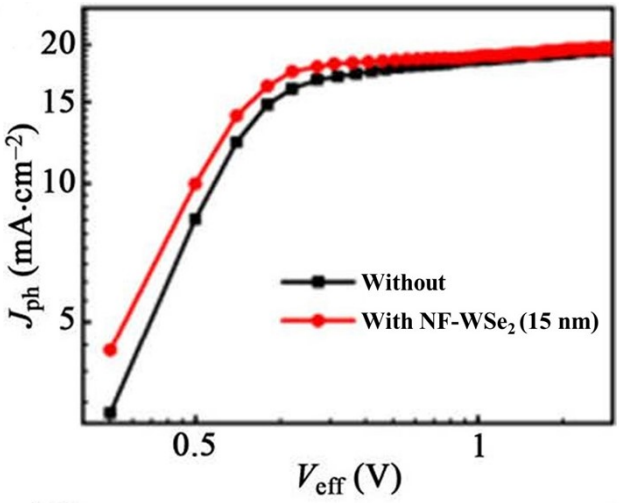

Fig. s10. J_{ph} versus V_{eff} curves of NF-WSe_2 devices.

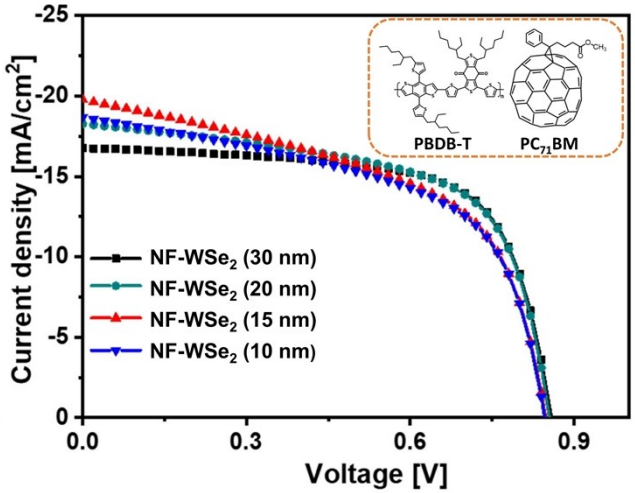

Fig. s11. *J–V* characteristics of PSCs made by PBDB-T:$PC_{71}BM$+bCar active layers with NF-WSe_2 for HTL at various spin-coated thicknesses.

Table s2. Summary of photovoltaic operating parameters for PBDB-T:$PC_{71}BM$+bCar PSCs made with different HTLs, measured under illumination of AM 1.5G (100 mW cm^{-2}).

Active layer	HTL	J_{sc} (mA cm^{-2})	V_{oc} (V)	*FF* (%)	PCE_{max} (PCE_{avg}) (%)
PBDB-T:PC71BM+bCar	NF-WSe_2 (10 nm)	16.8	0.84	56	8.2 (8.1±0.09)
	NF-WSe_2 (15 nm)	18.1	0.85	54	8.5 (8.3±0.17)
	NF-WSe_2 (20 nm)	19.6	0.85	55	9.2 (9.1±0.14)
	NF-WSe_2 (30 nm)	18.6	0.84	55	8.7 (8.5±0.15)

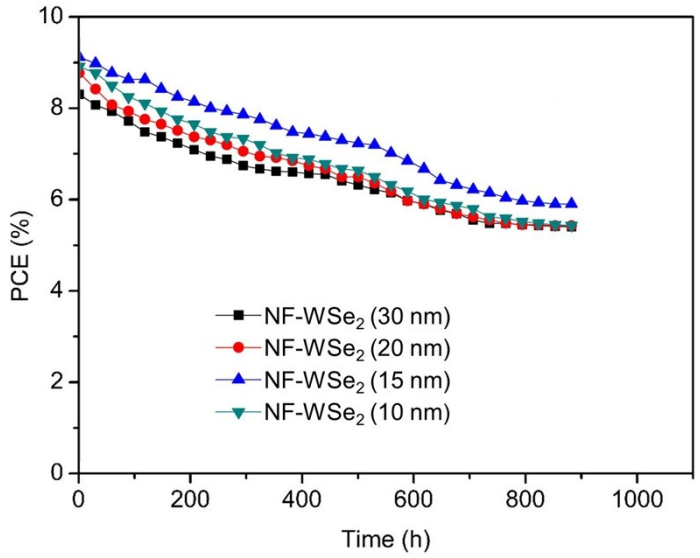

Fig. s12. Power conversion efficiency (PCE) of PBDB-T:$PC_{71}BM$+bCar-based PSCs with thickness-dependent NF-WSe_2 for HTL as a function of aging time.

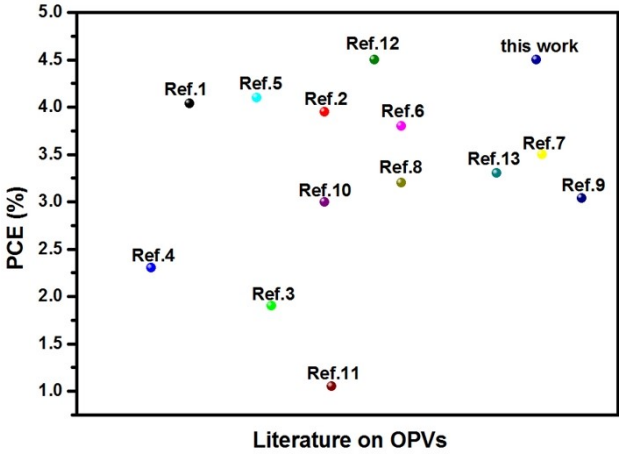

Fig. s13. A comparison of the performance with previously reported OPVs based on PCDTBT:PCBM BHJ.

Table s3. Comparison of the performance specifications of PCDTBT:PCBM BHJ solar cells in Fig. s9.

Acvie layer	HTL	Thickness of HTL (nm)	PCE (%)	V_{oc} (V)	J_{sc} (mA cm^{-2})	*FF* (%)	Resistance value (Ω)	Fatigue endurance	Ref.
PCDTBT:$PC_{60}BM$	PEDOT:PSS	30–40	4.04	0.904	7.7	58	Not shown	none	[1]
PCDTBT:$PC_{61}BM$	MoO_3		3.95	0.92	7.4	58	Not shown	none	[2]
PCDTBT:$PC_{71}BM$	MoO_3	20	1.9	0.57	8.69	38	Not shown	none	[3]
PCDTBT:$PC_{61}BM$			2.3	0.87	5.3	49	series resistance (R_s) is 50	none	[4]
PCDTBT:$PC_{61}BM$	MoO_3	3	4.1	0.871	7.8	60	Not shown	none	[5]
PCDTBT:PCBM-Ag NPs			3.8	0.853	7.3	67	Not shown	none	[6]
PCDTBT:$PC_{70}BM$	PEDOT:PSS with Pentacene	50	3.5	0.82	9.7	44	series resistance(R_s) is 19	none	[7]
P2:$PC_{60}BM$	PEDOT:PSS		3.2	0.78	9.31	44	Not shown	none	[8]
PCDTBT:$PC_{61}BM$ (PCB)2C2 (30%)	PEDOT:PSS		3.04	0.95	6.4	50	Not shown	none	[9]
PCDTBT:$PC_{61}BM$	PEDOT:PSS	20	3.0	0.75	8.53	43	Not shown	none	[10]
PCDTBT:$PC_{61}BM$ + PQT-12	PEDOT:PSS	40	1.05	0.562	5.62	33	Not shown	none	[11]
PCDTBT:$PC_{60}BM$	MoO_3	10	4.5				Not shown	PCE loss of 40% after 330 h	[12]
PCDTBT:$PC_{61}BM$	PEDOT:PSS	30	3.3	0.7	12.5	38	Not shown	Less than 40% of initial PCE after 1000h	[13]
PCDTBT:$PC_{71}BM$ +bCar	WSe_2	15	4.5	0.89	9.7	53.7	series resistance (R_s) is19; device resistance (R_d) is 244	Above 80% of initial PCE after 1000h	**This work**

Supporting references

[1] Aghassi A, Fay C D. Effects of IPA treatment on the photovoltaic performance of bulk heterojunction organic solar cells. Journal of Physics and Chemistry of Solids, 2019, 130: 136-143.

[2] Cai W, Zhong C, Duan C, et al. The influence of amino group on PCDTBT-based and P3HT-based polymer solar cells: Hole trapping processes. Applied Physics Letters, 2015, 106(23): 61.

[3] D'Olieslaeger L, Pfannmöller M, Fron E, et al. Tuning of PCDTBT: $PC_{71}BM$ blend nanoparticles for eco-friendly processing of polymer solar cells. Solar Energy Materials and Solar Cells, 2017, 159: 179-188.

[4] Clarke T M, Peet J, Nattestad A, et al. Charge carrier mobility, bimolecular recombination and trapping in polycarbazole copolymer: fullerene (PCDTBT: PCBM) bulk heterojunction solar cells. Organic Electronics, 2012, 13(11): 2639-2646.

[5] Mumyatov A V, Prudnov F A, Sagdullina D K, et al. Bis (pyrrolidino)[60] fullerenes: promising photostable fullerene-based acceptors suppressing light-induced absorber degradation pathways. Synthetic Metals, 2021, 271: 116632.

[6] Piralaee M, Ebrahimpour Z, Asgari A. The improved performance of BHJ organic solar cells by random dispersed metal nanoparticles through the active layer. Current Applied Physics, 2020, 20(4): 531-537.

[7] Sivakumar G, Pratyusha T, Gupta D, et al. Doping of hole transport layer PEDOT: PSS with pentacene for PCDTBT: PCBM based organic solar cells. Materials Today: Proceedings, 2017, 4(7): 6814-6819.

[8] Santos B P S, Lima A B, de Araujo F L, et al. Synthesis of novel low bandgap random and block terpolymers with improved performance in organic solar cells. Journal of Materials Research and

Technology, 2021, 10: 51-65.

[9] Schroeder B C, Li Z, Brady M A, et al. Enhancing Fullerene‐Based Solar Cell Lifetimes by Addition of a Fullerene Dumbbell. Angewandte Chemie, 2014, 126(47): 13084-13089.

[10] Etzold F, Howard I A, Mauer R, et al. Ultrafast exciton dissociation followed by nongeminate charge recombination in PCDTBT: PCBM photovoltaic blends. Journal of the American Chemical Society, 2011, 133(24): 9469-9479.

[11] Kumar A, Ratan S, Jarwal D K, et al. Effect of PQT-12 interface layer on the performance of PCDTBT: PCBM bulk heterojunction solar cells. Materials Research Express, 2019, 6(11): 115514.

[12] Li Z, Chiu K H, Ashraf R S, et al. Toward improved lifetimes of organic solar cells under thermal stress: Substrate-dependent morphological stability of PCDTBT: PCBM films and devices. Scientific reports, 2015, 5(1): 1-9.

[13] Ciammaruchi L, Oliveira R, Charas A, et al. Stability of organic solar cells with PCDTBT donor polymer: An interlaboratory study. Journal of Materials Research, 2018, 33(13): 1909-1924.